

The overlap between the thin- and thick-filament reflections in the small-angle X-ray diffraction pattern from a molluscan smooth muscle

Y. Tajima,^{a*} K. Makino,^b T. Hanyuu,^a K. Wakabayashi^c and Y. Amemiya^d

^aDepartment of Physics, Tokyo Metropolitan University, 1-1 Minami-Ohsawa, Hachioji, Tokyo 192-0397, Japan, ^bDepartment of Molecular Biology, Nagoya University, Chikusa-ku, Nagoya 464-8602, Japan, ^cDivision of Biophysical Engineering, Graduate School of Engineering Science, Osaka University, Toyonaka, Osaka 560-0043, Japan, and ^dDepartment of Applied Physics, Faculty of Engineering, University of Tokyo, Bunkyo, Tokyo 113-8656, Japan.
E-mail: tajima-yoshiko@c.metro-u.ac.jp

(Received 20 June 1998; accepted 23 November 1998)

Small-angle X-ray diffraction studies of the living anterior byssus retractor muscle (ABRM) of *Mytilus edulis* have been carried out using a long (2.2 m) point-focusing camera to investigate the overlap between the thin- and thick-filament reflections. While the reflections due to the cross-bridge lattice on the thick filaments in the resting ABRM are distant in the axial direction from the thin-filament layer lines, the paramyosin cores of the thick filaments produce reflections very close to the thin-filament reflections at axial spacings of 387, 59 and 51 Å. Using such a long camera it becomes possible to separate these reflections due to an improvement in the angular resolution and increase in the difference between the widths of the thin- and thick-filament reflections, and it is shown that the intensities of the 387 and 59 Å thin-filament layer lines gradually drop to zero close to the meridian. It becomes relatively easy to observe the thin-filament-based X-ray pattern by use of the long camera, making it possible to show a partial resemblance of the small-angle X-ray pattern from the contracting ABRM with the pattern from the rigorized ABRM.

Keywords: small-angle X-ray diffraction; molluscan smooth muscle; overlap between thin- and thick-filament reflections.

1. Introduction

X-ray diffraction is very useful for obtaining structural information on biological systems while they are functioning under intact physiological conditions. It offers important knowledge for studying the manner in which biological macromolecules interact with each other to produce specific functions. However, diffracted X-rays from biological systems are generally weak in intensity and appear at small diffraction angles corresponding to long and similar structural periods of many constituents. A change in the physiological state and the accompanying structural changes occur in a very short period of the order of 1 ms or less. Therefore, a well collimated thin and extremely strong X-ray beam is required for biological X-ray diffraction. An answer to this requirement was found in the application of synchrotron radiation from storage rings (Rosenbaum *et al.*, 1971; Holmes, 1974) and, nowadays, stable and high-brilliant synchrotron radiation has become indispensable to X-ray diffraction studies of biological systems.

Another requisite for biological applications of X-ray diffraction is the development of X-ray detectors which

have high sensitivity and high spatial resolution. In order to obtain intensity data before functional activity of the system is lowered by radiation damage, it is necessary to minimize the total flux to which the sample is exposed. New types of detector systems have been quickly introduced to X-ray diffraction experiments of muscle, which is the most typical example of a dynamical system (see review by Wakabayashi & Amemiya, 1991). One-dimensional position-sensitive detector systems have been extensively used for time-resolved small-angle X-ray diffraction of vertebrate striated muscle, and the collection of intensity data from contracting muscle with a time-resolution less than 1 ms has been realized (Huxley & Faruqi, 1983).

The small-angle X-ray diffraction pattern from the muscle shows fibre patterns from two kinds of protein filaments in the muscle cell, *i.e.* actin-containing thin filaments and myosin-containing thick filaments which are oriented in the direction of the length of the muscle. The central axes of the fibre pattern parallel and perpendicular to the filament axis are called the meridian and equator, respectively. In most cases, each of the fibre patterns consists of a set of layer-line reflections from individual filaments which occur in accordance with the periodicity of

the helical structure of the filaments. From the intensity change of the X-ray diffraction pattern due to transition of the muscle from the resting to contracting state, useful structural information is obtained for the study of the mechanism of the actin-myosin interaction that produces tension in contracting muscle. In order to analyse structural changes with high spatial resolution, it is necessary to collect time-resolved data of complete two-dimensional patterns. Wakabayashi *et al.* (1988) recorded two-dimensional X-ray diffraction patterns, including weak reflections, from contracting striated muscles using an imaging plate, an area-detector which has high sensitivity and high spatial resolution.

The authors have been studying structural changes in the thin and thick filaments during contraction of the anterior byssus retractor muscle (ABRM) of *Mytilus edulis* by small- and medium-angle X-ray diffraction using an imaging plate (Tajima *et al.*, 1994). In order to measure accurately the intensity change of the thin-filament-based pattern, X-ray diffraction of the ABRM with a long sample-to-detector distance, *i.e.* a long camera length, has been carried out in the present work.

Layer-line reflections from the thin filaments are clearly shown in the small-angle X-ray diffraction pattern from the ABRM (Vibert *et al.*, 1972) probably because the thin filaments are very long in the ABRM (Lowy & Hanson, 1962; Sobieszek, 1973). The periodic arrangement of myosin heads on the surface of the thick filaments in the resting ABRM does not seem to cause any detectable reflections in the area of the thin-filament reflections. These facts are favourable for intensity measurement of the X-ray diffraction pattern from the thin filaments, and for clarifying intensity changes of the pattern during contraction.

However, the thick filaments produce fine reflections on and near the meridian (Millman & Elliott, 1972; Lowy & Vibert, 1972) from the stems of the thick filaments, which are composed of a thick paramyosin core, and rod-shaped

parts of myosin molecules attached to the surface of the core (Lowy & Hanson, 1962; Sobieszek, 1973). Some of these reflections are very close to the thin-filament layer lines, and it is necessary to separate them to measure the intensities of the layer lines accurately. Therefore, in this work, an attempt is made to clarify the overlap between the reflections from the thin filaments and from the stems of the thick filaments by small-angle X-ray diffraction studies of the ABRM using a long camera length.

2. Materials and methods

Anterior byssus retractor muscles of ~ 30 mm in length were obtained from large specimens of *Mytilus edulis* (Tajima *et al.*, 1994). The muscle was teased down into a bundle of diameter 1 mm with a thin insect pin. The specimen was isometrically contracted at 281 K by stimulation with a strong acetylcholine solution (10^{-3} M) to produce high tensions (Fig. 1). Tonic tension, which was developed after the end of stimulation, was relaxed by application of 5-hydroxytryptamine (2.5×10^{-5} M).

X-ray diffraction experiments were carried out using synchrotron radiation and a point-focusing camera at beamline 15A of the Photon Factory, Tsukuba (Amemiya *et al.*, 1983). Small-angle X-ray diffraction patterns from the ABRM were recorded on 200×200 mm² (pixel size 0.1 mm \times 0.1 mm) imaging plates with 13 s exposure to an incident X-ray beam of intensity 5.2×10^{10} photons s⁻¹ mm⁻² using a camera length of 2.2 mm (*i.e.* as long as beamline 15A permits) (Amemiya *et al.*, 1988). The angular resolution was 0.36 mrad (4200 Å) in the 2.2 m camera. Higher-angle reflections outside the coverage of the imaging plate were observed by supplementary experiments with a 0.9 m camera.

Using the digital intensity data read from the imaging plate, the X-ray pattern was rotated and translated in order to make the meridian and the equator, respectively, parallel

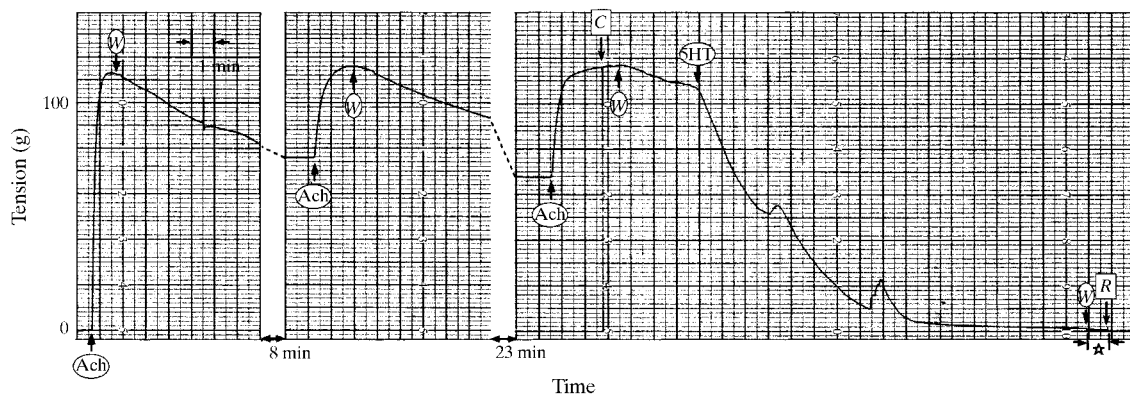


Figure 1

Tension record of a muscle bundle through the recording of the X-ray diffraction patterns shown in Fig. 2. Application of acetylcholine (ACh) and 5-hydroxytryptamine (5HT), as well as washing (W) them, are shown by the short arrows. The X-ray diffraction patterns in the contracting (C) and resting (R) states were taken at the positions shown by the long arrows. The pattern in the contracting state was taken after three stimuli when the tension reached a maximum (Twarog, 1967). The muscle bundle was set at the centre of the incident X-ray beam during the first two stimulations and the following slow relaxations (Tajima *et al.*, 1994). The muscle bundle generated a tension of 12.2 kg cm^{-2} during X-ray exposure in the contracting state. In the interval marked with the star, the chart speed was slowed down by a factor of 1/60.

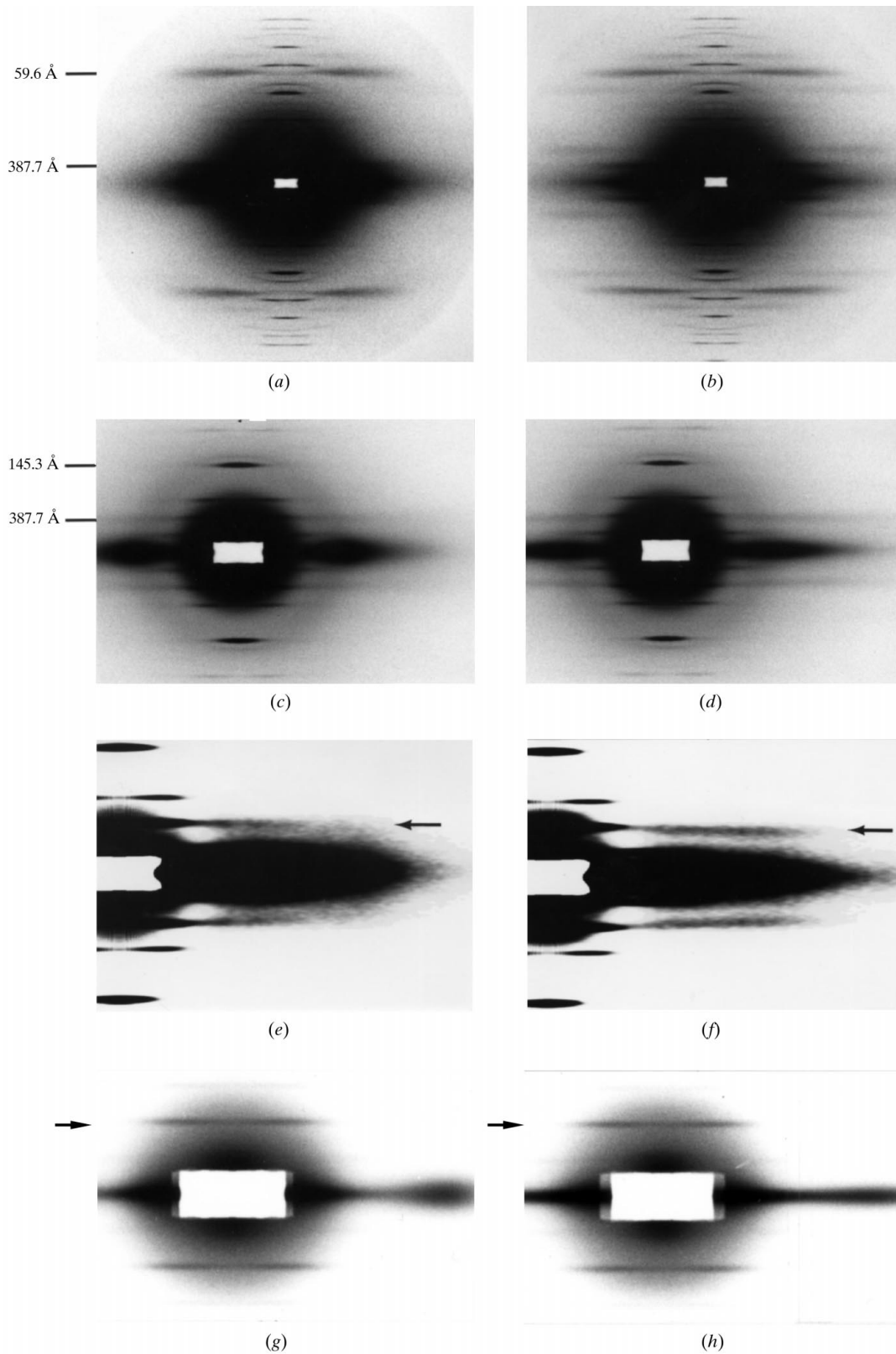


Figure 2

Small-angle X-ray diffraction patterns from the same part of an ABRM in the (a) resting and (b) contracting states recorded with the 2.2 m camera. The direction of length of the muscle is vertical. The central parts of the patterns (a) and (b) are reproduced at a high intensity level in (c) and (d), respectively, in order to show the 387 Å layer-line reflection from the thin filaments. It is shown more clearly in the background-subtracted patterns in the (e) resting and (f) contracting states. The arrows show the 387 Å layer line. Because a strong diffuse disc appears at the centres of the patterns (c) and (d), the patterns (g) and (h) are reproduced at a higher intensity level than the patterns (c) and (d) to show reflections in the diffuse disc. The arrows show the 363 Å layer line from the thick filaments.

to the axes of the pixel grid and for fitting the centre of the pattern to the centre of a pixel. Then the intensity data of the four quadrants were averaged. For comparison between the X-ray patterns in the resting and contracting states, the intensities of the patterns were brought to the same scale by adjusting the background intensities to the same level at a position far from the equator where the diffuse scattering from the ABRM almost diminished to zero (Poulsen & Lowy, 1983; Lowy & Poulsen, 1987). The entire background for subtraction from the X-ray pattern was calculated by third-order spline functions from the background data which were sampled at intervals of $6.91 \times 10^{-4} \text{ \AA}^{-1}$ (23 pixels) and 2.5° in the polar coordinates with the origin at the centre of the X-ray pattern. The background data were obtained from background curves fitted to points in between layer lines in tracings of the intensity distribution along the meridian.

3. Results

The X-ray patterns recorded with the 2.2 m camera show layer-line reflections from the thin filaments at axial spacings from 387 to 51 Å, and reflections from the thick filaments at axial spacings from 726 to 36 Å (Fig. 2). The thin- and thick-filament reflections observed in the resting state are schematically shown in Fig. 3. Here the term 'axial' means 'along the filament axis', and the axial spacing corresponds to the distance between the layer-line reflection and the equator, which is measured along the meridian. The observed axial spacings of the thin and thick filaments range up to 27 Å by adding higher-angle reflections which were recorded with the 0.9 m camera. Because the thin filaments are elongated more than the thick fila-

ments during contraction (Tajima *et al.*, 1994), relative axial positions of the thin- and thick-filament reflections are slightly changed by transition from the resting to the contracting state.

Comparing the X-ray diffraction patterns from the thick filaments in the resting and contracting states, the meridional reflections of low orders obviously change in intensity, but the intensities of the off-meridional reflections remain unchanged (Fig. 4). In the contracting state, the first meridional reflection (145 Å) is considerably weaker and the second (72 Å) is slightly stronger. The unchangeability in intensity of the off-meridional reflections agrees with a previous report by Lowy & Poulsen (1982) that no change was observed in intensity of the 360 Å reflection during contraction.

It is suggested by a rectangular model for the cross-bridge lattice on the thick filaments in the resting *Mytilus* ABRM (Squire, 1971) that the reflections from the myosin heads appear only on the layer lines which occur on the orders of the axial spacing, 145 Å, and that the primary reflection on each of the layer lines is a meridional reflection of the zeroth order of the Bessel function. Accordingly, it is considered that the intensity changes of the meridional thick-filament reflections during contraction are caused by a change in the myosin heads arrangement due to the movement of the myosin heads towards the thin filaments. On the other hand, intensities of the off-meridional thick-filament reflections are kept constant, probably because they entirely originate from the stems of the thick filaments which remain unchanged in structure during contraction.

In the X-ray diffraction patterns recorded with the 2.2 m camera, the reflections from the thin filaments are axially much broader than those from the thick filaments. The axial

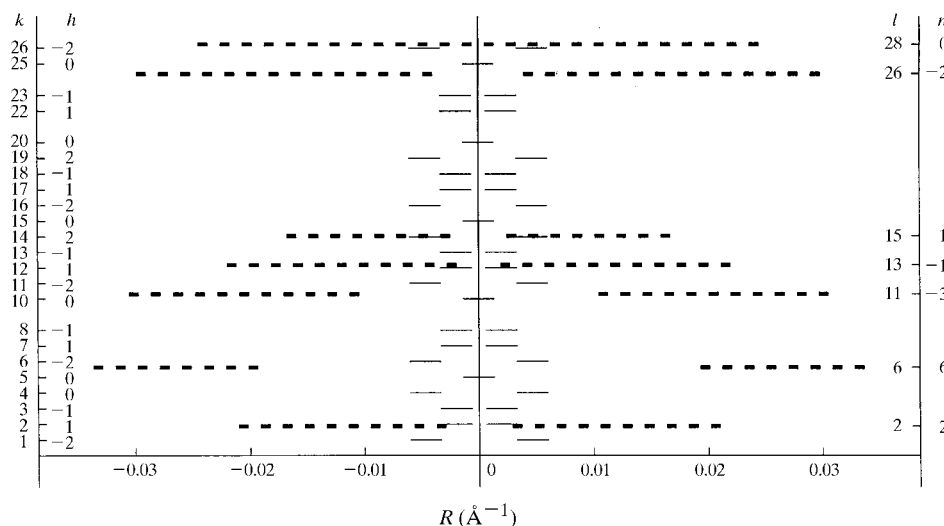


Figure 3

Schematic diagram of the layer-line reflections observed in the small-angle X-ray diffraction pattern from the resting ABRM. The abscissa R shows the radial (*i.e.* parallel to the equator) distance from the meridian in the reciprocal space. The long broken lines represent thin-filament reflections. The layer-line number l and the order of the Bessel function n shown on the right-hand scale are assigned on the basis of a 28/13 left-handed genetic helix of actin with a structural period of 775.4 Å (Tajima *et al.*, 1994). The short straight lines on and near the meridian represent the thick-filament reflections. The layer-line number k and the order of the Bessel function h shown on the left-hand scale are assigned after Bear & Selby (1956) with a structural period of 726.63 Å (Tajima *et al.*, 1994).

width of the thin-filament reflections increases with camera length with an incident X-ray beam kept converging to almost the same diameter on the imaging plate, while the axial width of the thick-filament reflections are unchanged by the change in the camera length (Figs. 2 and 5). Here, the axial width does not mean the angular width but means the size of the axial spread of the reflections on the imaging plate. The width of the thin-filament reflections is probably mainly determined by the correlation length between actin molecules, which depends on the degree of structural disorder of the thin filaments. On the other hand, the width of the thick-filament reflections is almost unaffected by structural disorder probably because of the high regularity of the thick-filament structure, but determined by the diameter of the incident beam. Because the diameter of the incident beam is unchanged, the angular resolution increases in proportion to the increase in the camera length. The improvement of the angular resolution straightforwardly appears in the unchangeability of the width of the thick-filament reflections, but has almost no effect on the width of the thin-filament reflections. Due to the diffraction properties of the thick filaments, it is possible to separate both reflections by using a long camera as discussed below. The thick-filament reflections will hereafter be called paramyosin reflections, because they mostly come from the paramyosin cores, especially the off-meridional reflections.

As shown in Fig. 3, the second (363 Å), 12th (60 Å), 14th (51 Å) and 26th (27 Å) paramyosin reflections are axially very close to the second (387 Å), 13th (59 Å), 15th (51 Å) and 28th (27 Å) layer lines, respectively, from the thin filaments. The differences between the diffraction angles along the meridian of the first and second pairs of the

paramyosin and thin-filament reflections are comparable with the angular resolution of the 2.2 m camera. In each of the third and fourth pairs, the difference between the diffraction angles of the paramyosin and thin-filament reflections is smaller than the angular resolution. However, the paramyosin reflection can be distinguished from the thin-filament reflection due to a remarkable difference in their widths, making it probable to separate the two reflections. Among the four pairs of reflections, the third pair of the 14th paramyosin reflection and the 15th thin-filament reflection is the closest. The difference between the diffraction angles of these reflections along the meridian is 0.0068° , and the corresponding distance on the imaging plate amounts to 0.26 mm in the long camera. This distance is large enough to be resolved on an imaging plate of pixel size $0.1 \text{ mm} \times 0.1 \text{ mm}$.

The 12th paramyosin reflection and the 13th thin-filament reflection are obviously separated in the patterns recorded with the long camera (Figs. 2, 6 and 7) as in the X-ray diffraction pattern from the ABRM fixed with glutaraldehyde (Lowy & Vibert, 1972). As a result of separation of the 12th paramyosin reflection, it is shown in the pattern from the contracting ABRM that the intensity of the 13th thin-filament layer line gradually drops to zero with a decrease in the distance from the meridian. In the pattern from the resting ABRM, a very weak intensity is detected at the meridian on the 13th layer line, but it may be regarded as a pseudo-meridional reflection deriving from tilted filaments due to incomplete orientation of the thin filaments.

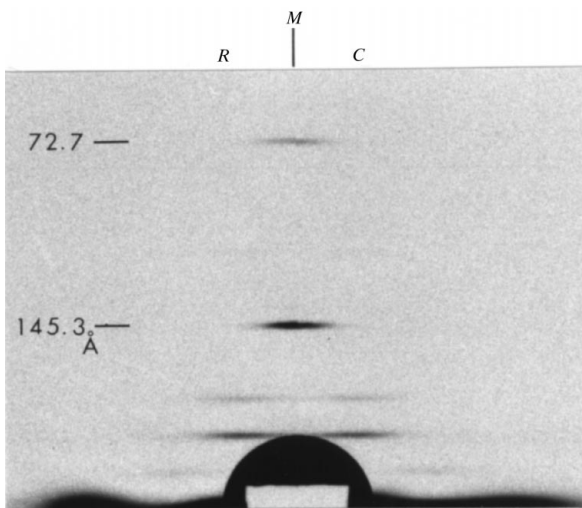


Figure 4
Comparison between the thick-filament-based X-ray patterns from the same part of an ABRM in the resting and contracting states. The left and right sides of the meridian (*M*) show the background-subtracted X-ray patterns from the resting (*R*) and contracting (*C*) ABRM, respectively. The first- and second-order meridional reflections of the 145 Å repeat are shown.

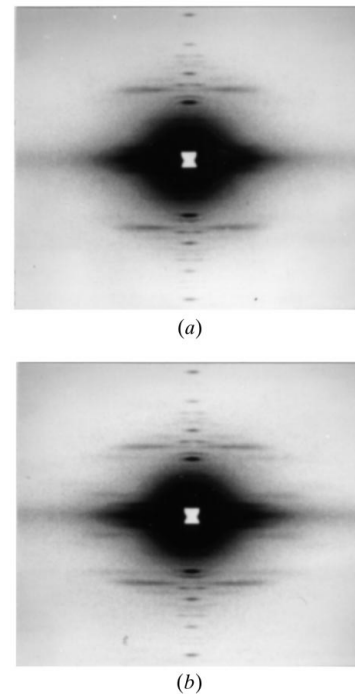


Figure 5
Small-angle X-ray patterns from the same part of an ABRM in the (a) resting and (b) contracting states which were recorded with a 0.9 m camera.

Figs. 2(c) and 2(d) show the overlap between the second (387 Å) thin-filament layer-line reflection and the second (363 Å) paramyosin reflection that occurs at the end of the former reflection closer to the meridian (Fig. 3). Because the 387 Å layer line is broader and nearer to the equator than the 363 Å layer line, it is recognized that the intensity of the second layer line from the thin filaments gradually drops with decrease in the distance from the meridian (Figs. 2e and 2f). No trace of the second layer line from the thin filaments is detected in the central diffuse disc (Lowy & Poulsen, 1982) (Figs. 2g and 2h). A detailed examination of the X-ray patterns on a computer display also indicates that the intensity of the second layer line from the thin filaments drops to zero on and very near the meridian.

The 14th (51 Å) paramyosin reflection is so close to the 15th (51 Å) thin-filament reflection that it is completely overlaid by the latter. However, the existence of the paramyosin reflection can be recognized because the

paramyosin reflection is axially sharper than the thin-filament reflection, and the relative axial positions of the two reflections are changed during contraction. The 14th paramyosin reflection along the lower edge of the 15th thin-filament reflection in the resting state is seen along the upper edge of the 15th thin-filament reflection during contraction (Fig. 6). Intensity distributions across the layer lines show the change in the relative axial positions of the two reflections (Figs. 7a and 7c).

Because the 26th (27 Å) paramyosin reflection and the 28th (27 Å) thin-filament reflection are axially more distant in the resting state than the three pairs of paramyosin and thin-filament reflections described above, it is possible to recognize the existence of the 26th paramyosin reflection in the X-ray diffraction pattern recorded with the 0.9 m camera. Although the two reflections become closer to each other in the contracting state, the 26th paramyosin reflection is seen as a spot on the 28th thin-filament

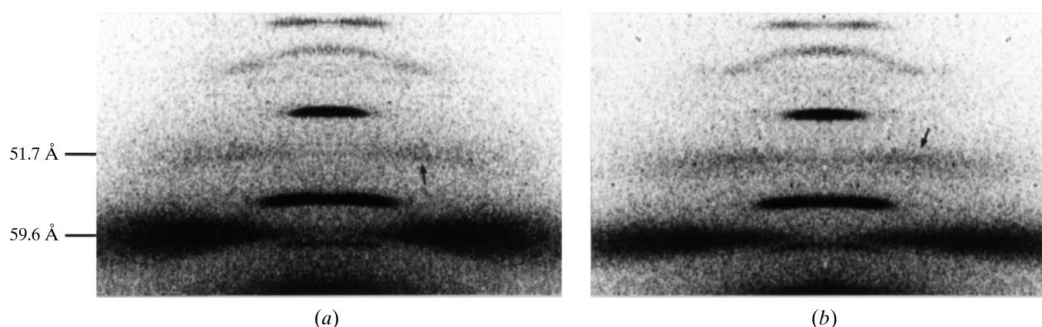


Figure 6

Partially magnified X-ray patterns from an ABRM in the (a) resting and (b) contracting states which show the area of 59 and 51 Å thin-filament layer-line reflections. The patterns are axially magnified by a factor of two radially. The arrows show the 51 Å paramyosin reflection ($k = 14$, $h = 2$) overlaid by the 51 Å thin-filament reflection ($l = 15$, $n = 1$).

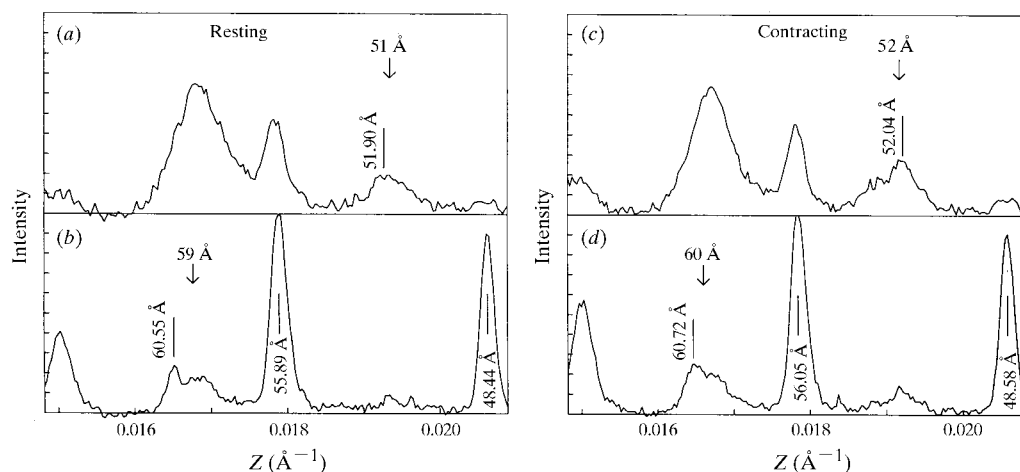


Figure 7

Background-subtracted axial intensity profiles in the resting and contracting states that were obtained by radial integration of the intensities within the region 2.5×10^{-3} – $7.3 \times 10^{-3} \text{ Å}^{-1}$ (a and c) where the paramyosin reflections of the second-order Bessel function are seen, and the region 0 – $3.2 \times 10^{-3} \text{ Å}^{-1}$ (b and d) where the paramyosin reflections of the first-order Bessel function are seen. The abscissa Z shows the axial distance from the equator in the reciprocal space. The vertical bars show reflections from the thick filaments, and the arrows show the 51 and 59 Å reflections from the thin filaments. The spacings of these reflections are slightly elongated during contraction. The profiles in (a) and (c) show an overlap between the 15th (51 Å) thin-filament reflection and the 14th (51 Å) paramyosin reflection, and those in (b) and (d) show neighbouring peaks of the 13th (59 Å) thin-filament reflection and the 12th (60 Å) paramyosin reflection.

reflection because of an intensity decrease of the latter reflection (Tajima & Amemiya, 1991).

Using the long camera it becomes relatively easy to observe weak reflections which appear, during contraction, under the 59 Å layer line in accordance with the structural repeat of the thin filament (Tajima *et al.*, 1994). Comparing the background-subtracted patterns from the ABRM in the resting and contracting states, it is found that weak, but new, reflections appear during contraction at axial spacings 70 ($l = 11$), 86 ($l = 9$), 110 ($l = 7$) and 193 Å ($l = 4$) (Figs. 8 and 9). The reflections at spacings 86 and 110 Å are similar to those observed by Lowy & Vibert (1972) in the tonically contracting ABRM. The 110 Å reflection seems to overlap with a subsidiary peak of the 103 Å (seventh) paramyosin reflection in a position close to the meridian.

Although the four reflections that appear under the 59 Å layer line during contraction are axially on the orders of the structural repeat of the thin filament, they are radially closer to the meridian than those predicted from the thin-filament structure composed of actin and tropomyosin. These reflections seem to appear in connection with the well known intensity increase of the 193 Å layer line which occurs relatively far from the meridian about the radial position, 0.02 \AA^{-1} , as a result of activation of the thin

filaments (Vibert *et al.*, 1972; Tajima & Amemiya, 1991). The intensities of the four reflections are approximately in proportion to the intensity of this 193 Å reflection. Even when the specimen spontaneously produces a tension (Lowy & Millman, 1963) as small as 5% of the maximum tension produced by stimulation with $10^{-3} M$ acetylcholine, a tension that is so small that the specimen seems as if it is in the resting state, the 70 and 86 Å reflections are faintly seen, together with a weak 193 Å reflection about the radial position, 0.02 \AA^{-1} .

Intensity distributions along the 387, 59 and 51 Å layer lines from the thin filaments, which are obtained by axial integration within the width of the layer-line reflections, change during contraction. The 387 and 51 Å layer lines increase and the 59 Å layer line decreases in integrated intensity in the part close to the meridian (Tajima *et al.*, 1994). These intensity changes are illustrated in Fig. 9 together with the four reflections described above. The diagram shows a pattern that resembles the X-ray diffraction pattern from the ABRM in the rigor state (Lowy & Vibert, 1972; Tajima, 1982). The rigor pattern recorded in this work is shown in Fig. 10. It is supposed that the myosin heads interact with the thin filaments at a specific site of actin during some steps of tension generation, and that the thin filaments are partially and temporarily decorated with these myosin heads. The intensity decrease in the 59 Å layer line probably results from a phase difference between the scattering amplitudes from the actin helix and the myosin heads.

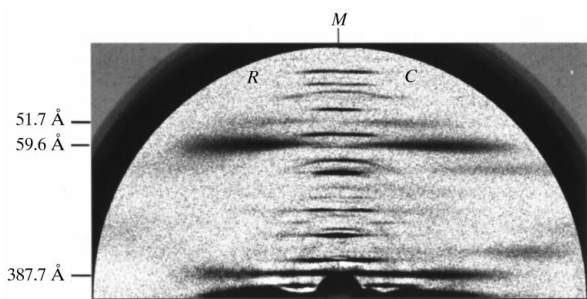


Figure 8

Comparison between the background-subtracted X-ray patterns from the same part of an ABRM in the resting and contracting states. The left and right sides of the meridian (M) show the patterns from the resting (R) and contracting (C) ABRM, respectively.

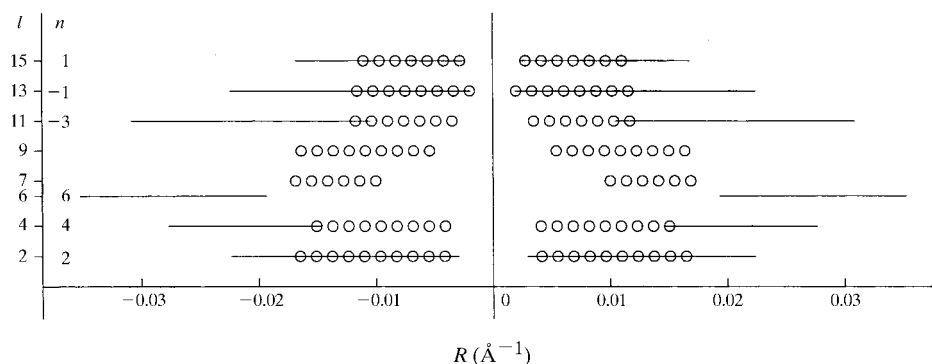


Figure 9

Schematic diagram of the X-ray pattern from the thin filament in the contracting state. Although the symmetry of actin helix may be slightly modified during contraction (Wakabayashi *et al.*, 1994), the layer lines are indexed for approximation to an actin helix of 28/13 symmetry in the resting muscle. The intensity changes that occur near the meridian during contraction are shown by rows of open circles.

4. Summary

The overlap between the reflections from the thin and thick filaments was clarified by recording small-angle X-ray patterns from the ABRM with a long (2.2 m) camera. Because the thick-filament reflections are relatively narrow in axial width compared with the thin-filament reflections, it is possible to separate the second (387 Å), 13th (59 Å) and 15th (51 Å) thin-filament layer-line reflections from the second (363 Å), 12th (60 Å) and 14th (51 Å) paramyosin

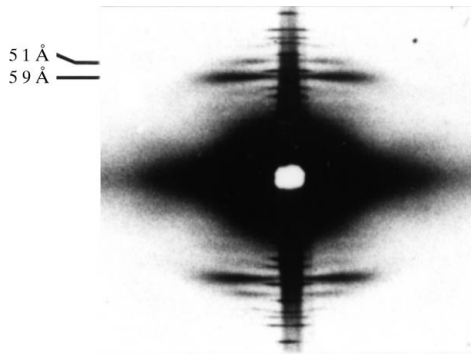


Figure 10

A small-angle X-ray diffraction pattern from a glycerinated ABRM in the rigor state which had been recorded on X-ray film before imaging plates became available. The ABRM was glycerinated by the method of Baguet (1973), and the X-ray pattern was taken by a rotating-anode microfocusing X-ray generator operated at 40 kV and 15 mA (nominal focal size $0.1 \text{ mm} \times 0.1 \text{ mm}$) and a mirror-monochromator point-focusing camera with a camera length of 0.25 m. The exposure time was 75 h. The pattern shows a ladder-like appearance of the layer-line reflections from the thin filaments involving 51 and 59 Å layer lines, and three layer lines under the 59 Å layer line, similar to the rigor patterns from striated muscles (Wakabayashi & Amemiya, 1991).

reflections, respectively. It was shown that the intensities of the second and 13th layer lines from the thin filaments gradually drops to zero close to the meridian. The overlap between the 28th (27 Å) thin-filament layer line and the 26th (27 Å) paramyosin reflection was observed in the X-ray patterns recorded with a 0.9 m camera.

The use of the long camera length also improved the separation between the layer lines from the thin filaments, making it easy to observe weak reflections that appear under the 59 Å layer line during contraction. It was shown that the X-ray diffraction pattern from the contracting ABRM partially resembles the pattern from the rigorized ABRM.

This work has been performed under the approval of the Photon Factory Program Advisory Committee (Proposal No. 94-G080).

References

- Amemiya, Y., Matsushita, T., Nakagawa, A., Satow, Y., Miyahara, J. & Chikawa, J. (1988). *Nucl. Instrum. Methods*, **A266**, 645–653.
- Amemiya, Y., Wakabayashi, K., Hamanaka, T., Wakabayashi, T., Matsushita, T. & Hashizume, H. (1983). *Nucl. Instrum. Methods*, **208**, 471–477.
- Baguet, F. (1973). *Pflügers Arch.* **340**, 19–34.
- Bear, R. S. & Selby, C. C. (1956). *J. Biophys. Biochem. Cytol.* **2**, 55–69.
- Holmes, K. C. (1974). *Endeavour*, **33**, 60–66.
- Huxley, H. E. & Faruqi, A. R. (1983). *Ann. Rev. Biophys. Bioeng.* **12**, 381–417.
- Lowy, J. & Hanson, J. (1962). *Physiol. Rev.* **42**, 34–42.
- Lowy, J. & Millman, B. M. (1963). *Philos. Trans. R. Soc. B*, **246**, 105–148.
- Lowy, J. & Poulsen, F. R. (1982). *Nature (London)*, **299**, 308–312.
- Lowy, J. & Poulsen, F. R. (1987). *J. Mol. Biol.* **194**, 595–600.
- Lowy, J. & Vibert, P. J. (1972). *Cold Spring Harb. Symp. Quant. Biol.* **37**, 353–359.
- Millman, B. M. & Elliott, G. F. (1972). *Biophys. J.* **12**, 1405–1414.
- Poulsen, F. R. & Lowy, J. (1983). *Nature (London)*, **303**, 146–152.
- Rosenbaum, G., Holmes, K. C. & Witz, J. (1971). *Nature (London)*, **230**, 434–437.
- Sobieszek, A. (1973). *J. Ultrastruct. Res.* **43**, 313–343.
- Squire, J. M. (1971). *Nature (London)*, **233**, 457–462.
- Tajima, Y. (1982). Unpublished.
- Tajima, Y. & Amemiya, Y. (1991). *Adv. Biophys.* **27**, 77–88.
- Tajima, Y., Makino, K., Hanyuu, T., Wakabayashi, K. & Amemiya, Y. (1994). *J. Muscle Res. Cell Motil.* **15**, 659–671.
- Tajima, Y., Wakabayashi, K. & Amemiya, Y. (1994). *Synchrotron Radiation in the Biosciences*, edited by B. Chance, J. Deisenhofer, S. Ebashi, D. T. Goodhead, J. R. Helliwell, H. E. Huxley, T. Iizuka, J. Kirz, T. Mitsui, E. Rubinstein, N. Sakabe, T. Sasaki, G. Schmahl, H. B. Stuhmann, K. Wüthrich & G. Zaccai, pp. 509–518. Oxford University Press.
- Twarog, B. M. (1967). *J. Physiol.* **192**, 847–856.
- Vibert, P. J., Haselgrove, J., Lowy, J. & Poulsen, F. R. (1972). *J. Mol. Biol.* **71**, 757–767.
- Wakabayashi, K. & Amemiya, Y. (1991). *Handbook on Synchrotron Radiation*, edited by S. Ebashi, M. Koch & E. Rubenstein, pp. 597–678. Amsterdam: Elsevier.
- Wakabayashi, K., Sugimoto, Y., Tanaka, H., Ueno, Y., Takezawa, Y. & Amemiya, Y. (1994). *Biophys. J.* **67**, 2422–2435.
- Wakabayashi, K., Ueno, Y., Amemiya, Y. & Tanaka, H. (1988). *Molecular Mechanism of Muscular Contraction*, edited by H. Sugi & G. H. Pollack, pp. 353–367. New York: Plenum.